

Wigner Localization in a Graphene Quantum Dot with a Mass Gap

K. A. Guerrero Becerra

*CNR-NANO Research Center S3, Via Campi 213/a, 41125 Modena, Italy
Università degli Studi di Modena and Reggio Emilia, Italy*

Massimo Rontani

*CNR-NANO Research Center S3, Via Campi 213/a, 41125 Modena, Italy**

We show that Dirac electrons in a graphene quantum dot with a mass gap localize à la Wigner for realistic values of device parameters. Our theoretical evidence relies on many-body energies, one-body densities, and pair correlation functions obtained through the exact diagonalization of the interacting Hamiltonian, which allows us to take all many-body correlations into account. We predict that the experimental signatures of Wigner localization are the suppression of the fourfold periodicity of the filling sequence and the quenching of excitation energies, which may be both accessed through Coulomb blockade spectroscopy.

PACS numbers: 73.22.Pr, 73.21.La, 31.15.ac, 73.20.Qt

The role of electron-electron interactions in graphene is a fundamental and yet open issue [1–4] that impacts on the operation of quantum dots (QDs) [5–7] and other graphene-based nanodevices [6, 8–11]. Since the density of states vanishes at the charge neutrality point, making Coulomb interaction unscreened, one might expect strongly correlated behavior at low energies. Indeed, the fine structure constant α —the ratio of Coulomb to Fermi energy—is of order unity, much larger than the value $\alpha = 1/137$ of quantum electrodynamics, therefore the many-body problem may not be treated with perturbative methods. As a matter of fact, the predicted ratio of viscosity to entropy per electron is characteristic of an extremely interacting quantum fluid [12].

However, electrons in bulk graphene allegedly behave as noninteracting particles, except for subtle effects due to velocity renormalization [13–15], coupling with phonons / plasmons [16], and a hypothetical excitonic gap [17, 18]. The key to this paradox is that the density parameter r_s , which quantifies the impact of electron correlations [19], does not depend on the electron density n but coincides with α [20]. In contrast, $r_s \sim n^{-1/2}$ of the conventional two-dimensional electron gas [21] increases as n decreases due to the massive dispersion of electrons. An electron solid (Wigner crystal) is even predicted in the dilute limit [22], as the long-range order induced by Coulomb interaction localizes electrons in space. Therefore, a way to disclose the many-body physics of graphene is to make electrons massive, invalidating the above scaling argument. This occurs e.g. in the fractional quantum Hall effect [23, 24] and in bilayer graphene [25], which might be an excitonic insulator [26].

In this Letter we explore theoretically the few-body physics of a graphene QD with a mass gap. Our motivation is twofold: On one side, electrons in semiconductor QDs may form Wigner molecules [27–30], i.e., finite-size precursors of the Wigner crystal, including carbon-based nanostructures—nanotubes—for which the effect

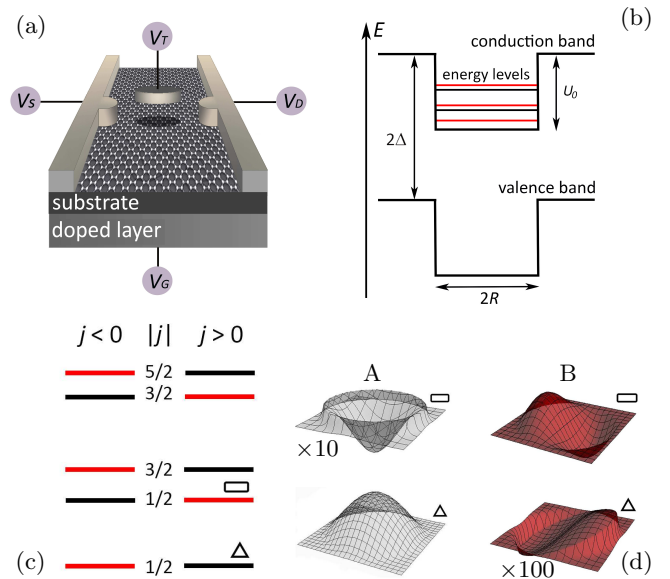


Figure 1. (color online) Graphene QD defined by electrostatic gates. (a) Proposed setup. The top gate (V_T) defines the dot while source (V_S), drain (V_D), and back (V_G) gates allow for Coulomb blockade spectroscopy. (b) Radial QD confinement potential. The interaction between graphene and substrate opens a mass gap 2Δ in the QD energy spectrum. (c) Lowest noninteracting QD energy levels in the conduction band. Black (red [gray]) lines label states in K (K') valley. (d) Real part of sublattice-resolved envelopes whose energies are labeled by the square and triangle symbols in panel c.

is dramatic [31]. On the other side, a current trend in graphene QDs is to minimize the roles of disorder and edge states, which are extrinsic sources of localization. These next-generation devices include atomically precise nanoribbons [10, 32] and bilayer QDs—possibly defined through gates [33–36].

Here we consider a clean, circular QD with a mass gap induced by the breaking of sublattice symmetry. This could be realized through the interaction between

graphene and substrate [37], such as BN [38–40] and SiC [41] (but the evidence for these materials is debated [40, 42–47]). The presence of the gap allows to electrostatically define the QD as well as to perform Coulomb blockade spectroscopy, as sketched in Figs. 1(a)-(b).

Other authors already suggested that electrons in graphene QDs may crystallize. However, some of these analyses were limited to degenerate edge states that are sensitive to interactions as well as to all kinds of perturbation [48–51], whereas other theories treated Coulomb interaction at the mean field level [52], which may artificially enhance localization [27], or considered only valley-polarized electrons [53], which artfully breaks time-reversal symmetry. Here we exactly diagonalize the full interacting Hamiltonian taking into account correlations at all orders and the presence of inequivalent K (isospin $\tau = 1$) and K' ($\tau = -1$) Dirac cones. Through the analysis of the energy spectrum, charge density and pair correlation functions we show that electrons form Wigner molecules in realistic devices, exhibiting signatures of crystallization in Coulomb blockade spectra.

The envelope-function QD Hamiltonian for noninteracting electrons in the valley τ [37] is

$$\hat{H}_\tau = -i\hbar v_F (\hat{\tau}_1 \partial/\partial x + \hat{\tau}_2 \partial/\partial y) + \tau \Delta \hat{\tau}_3 + U(\rho) \hat{\tau}_0. \quad (1)$$

Here $v_F \approx 10^6$ m/s is the Fermi velocity, the 2×2 Pauli matrices $\hat{\tau}_1, \hat{\tau}_2, \hat{\tau}_3$, and the unit matrix $\hat{\tau}_0$ act on pseudospinors whose components are the A/B sublattice envelopes, $U(\rho) = U_0 \Theta(\rho - R)$ is the circular hard-wall confinement potential of height U_0 plotted in Fig. 1(b), with R being the QD radius and $\rho = (x^2 + y^2)^{1/2}$. The potential U , modulated by the top gate shown in Fig. 1(a), confines the electrons in the QD since the Zeeman-like term $\Delta \hat{\tau}_3$ breaks sublattice inversion symmetry, hence inducing a gap 2Δ into the energy spectrum [Fig. 1(b)]. In the following we take $\Delta = U_0 = 0.26$ eV.

We find numerically the eigenvalues of \hat{H}_τ following the method of [37]. The QD bound states $\Phi(\mathbf{r})$ are pseudospinors of the form

$$\Phi(\mathbf{r}) = e^{i(j-1/2)\varphi} \begin{pmatrix} \mathcal{R}^A(\rho) \\ e^{i\varphi} \mathcal{R}^B(\rho) \end{pmatrix}, \quad (2)$$

where φ is the azimuthal angle, $j = \pm 1/2, \pm 3/2, \dots$ is the half-integer quantum number eigenvalue of the total angular momentum $\hat{j}_z = -i\hbar \partial/\partial \varphi + \hbar \hat{\tau}_3/2$, and $\mathcal{R}^A(\rho)$ is the radial envelope on sublattice A [54]. As illustrated in Fig. 1(c) for the lowest conduction-band states, QD orbitals whose quantum numbers differ solely in the sign of τ (black or red [gray] lines) have different energies since inversion symmetry is broken, whereas time reversal symmetry protects $\varepsilon(\tau, j) = \varepsilon(-\tau, -j)$. Overall, including the spin degree of freedom $\sigma = \uparrow, \downarrow$, QD levels are four-fold degenerate. Both radial profiles and integrated weights of envelopes $\mathcal{R}(\rho)$ are generically different on the two sublattices, as shown in the example of Fig. 1(d).

We consider a few excess interacting charge carriers populating the QD conduction band. The presence of the gap 2Δ allows us to ignore the pathologies that plague the many-body problem of Dirac electrons due to the unboundedness of the energy spectrum [55, 56]. The interacting Hamiltonian is

$$\hat{H} = \sum_{a\tau\sigma} \varepsilon_{a\tau} \hat{c}_{a\tau\sigma}^\dagger \hat{c}_{a\tau\sigma} + \frac{1}{2} \sum_{abcd} \sum_{\tau\tau'} \sum_{\sigma\sigma'} \times \langle a\tau, b\tau' | v(\mathbf{r} - \mathbf{r}') | c\tau', d\tau \rangle \hat{c}_{a\tau\sigma}^\dagger \hat{c}_{b\tau'\sigma'}^\dagger \hat{c}_{c\tau'\sigma'} \hat{c}_{d\tau\sigma}, \quad (3)$$

where $\hat{c}_{a\tau\sigma}^\dagger$ creates an electron of spin σ in the orbital $|a\tau\rangle$ labeled by quantum numbers τ and $a \equiv (j_a, n_a)$ whose energy is $\varepsilon_{a\tau}$ (n_a is the number of radial nodes). Two-body interaction takes the Ohno form $v(\mathbf{r} - \mathbf{r}') = v_0 [1 + (v_0 \epsilon / e^2)^2 |\mathbf{r} - \mathbf{r}'|^2]^{-1/2}$, where ϵ is the background relative dielectric constant. Since realistic values of ϵ fall in a wide range between $\epsilon = 1.4$ and $\epsilon = 44$, depending on the substrate [57, 58] as well as on nearby gates, here we treat ϵ as a free parameter. At large distances v approaches the Coulomb potential, whereas its contact limit is the Hubbard-like intra-atomic interaction $v_0 = 15$ eV for the $2p_z$ orbital [59]. Matrix elements $\langle a\tau, b\tau' | v | c\tau', d\tau \rangle$ are obtained from tight-binding states neglecting interatomic orbital overlaps [60] as well as small intervalley exchange terms [61].

The many-body states are superpositions of the Slater determinants obtained by filling the lowest 68 spin-valley-orbitals with N electrons in all possible ways (aka full configuration interaction [62]), which ensures convergence. In this Fock basis \hat{H} is a sparse matrix, with blocks labeled by the total angular momentum and (iso)spin. The maximum linear size of the matrix is 2,187,712, which we diagonalize with the home-built parallel code DONRODRIGO [29–31, 62]. This provides highly accurate energies and wave functions of both ground and excited states, in contrast to other high-level methods, such as quantum Monte Carlo, addressing ground state properties only.

A key quantity we obtain from the computed ground state energies $E_0(N)$ is the chemical potential $\mu(N) = E_0(N) - E_0(N-1)$, that is the resonating tunneling energy of the N th electron injected into the QD containing $N-1$ interacting particles. This may be measured through Coulomb blockade spectroscopy, as electrons are added to the QD one by one tuning the backgate shown in Fig. 1(a) [63]. In Fig. 2 we artificially modulate the background screening ϵ to highlight the effect of Coulomb interaction on the filling sequence (here $R = 250$ Å). In the absence of interactions ($\epsilon = 100$, dotted line), $\mu(N)$ is constant except for a step when adding the fifth electron, which corresponds to a peak in the charging energy $\Delta\mu(N) = \mu(N+1) - \mu(N)$ (see inset). This finite value $\Delta\mu(N=4) \approx 10$ meV is the orbital energy cost required to add an electron to the second shell after the first one has been filled with four electrons. This fourfold period-

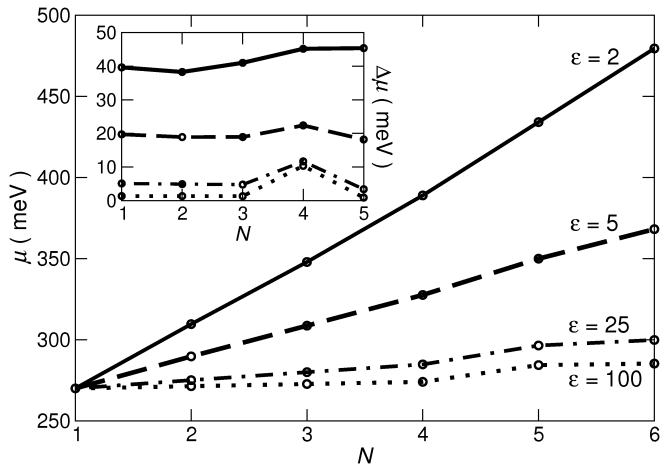


Figure 2. Coulomb blockade linear spectroscopy. Chemical potential $\mu(N)$ vs N for different background dielectric constants ϵ , with $R = 250$ Å. Inset: Charging energy $\Delta\mu(N)$ vs N . Lines are guides to the eye.

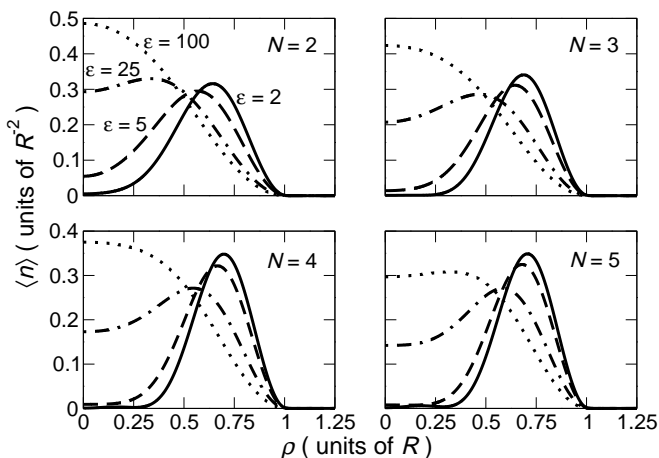


Figure 3. Emergence of radial correlations in the wave function. One-body density $\langle n(\mathbf{r}) \rangle$ vs ρ for different values of ϵ and N , with $R = 1250$ Å.

icity is generic for all fillings, as clear from Fig. 1(c).

As the interaction strength is turned on, the shell structure of $\mu(N)$ is progressively washed out. In contrast with circular QDs in ordinary semiconductors [64], the charging energy $\Delta\mu$ shown in the inset of Fig. 2 neither exhibits half-shell peaks linked to Hund's rule nor decreases with N . The former feature, shared by carbon-nanotube QDs [31, 65], is due to the spin-valley multi-component nature of the wave function, while the latter is peculiar to the hard-wall confinement potential. For realistic values of ϵ the Coulomb energy overwhelms the kinetic energy, making μ increase almost linearly with N (dashed and solid lines for $\epsilon = 5$ and 2 , respectively).

To clarify how interactions affect the wave function we

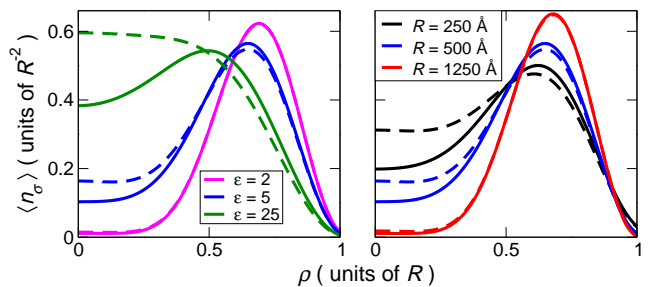


Figure 4. (color online). Suppression of exchange interactions. Spin-resolved density $\langle n_\sigma(\mathbf{r}) \rangle$ vs ρ for different values of ϵ (left panel, $R = 500$ Å) and R (right panel, $\epsilon = 5$), with $N = 5$ and $S_z = 1/2$. Solid and dashed lines point to $\langle n_\uparrow \rangle$ and $\langle n_\downarrow \rangle$, respectively.

compute the—circularly symmetric—one-body density

$$\langle n(\mathbf{r}) \rangle = \frac{1}{N} \sum_{i=1}^N \langle \delta(\mathbf{r} - \mathbf{r}_i) \rangle, \quad (4)$$

where $\langle \dots \rangle$ is the quantum statistical average for vanishing temperature. In practice, we average $\langle n(\mathbf{r}) \rangle$ over the ground-state multiplet, whose large angular-momentum degeneracy is protected by symmetry against the effect of interaction. After the averaging $\langle n(\mathbf{r}) \rangle$ is the same on both sublattices, unspecified in the following.

Figure 3 shows the evolution of the radial profile of $\langle n(\mathbf{r}) \rangle$ with the interaction strength. Whereas for large screening (dotted lines) the probability weight is spread all over the QD, as ϵ is decreased the central region is depleted with its weight being moved towards the dot wall. For realistic screening (dashed and solid lines) $\langle n \rangle$ is a ring with electrons pushed against the potential wall by Coulomb repulsion, which hints to the formation of a Wigner molecule [27]. This trend is generic for different electron numbers and dot radii, the larger R the higher ϵ at which the ring structure sets in (data not shown).

A fingerprint of Wigner localization is provided by the spin-resolved one-body density $\langle n_\sigma(\mathbf{r}) \rangle$,

$$\langle n_\sigma(\mathbf{r}) \rangle = \frac{1}{N_\sigma} \sum_{i=1}^N \langle \delta_{\sigma\sigma_i} \delta(\mathbf{r} - \mathbf{r}_i) \rangle_{S_z}. \quad (5)$$

Here N_σ is the number of electrons with spin σ so $\langle n_\sigma(\mathbf{r}) \rangle$ is normalized to one, and $\langle \dots \rangle_{S_z}$ is the average taken over the manifold of states with fixed total spin projection $S_z = (N_\uparrow - N_\downarrow)/2$. For odd electron numbers $\langle n_\uparrow(\mathbf{r}) \rangle$ and $\langle n_\downarrow(\mathbf{r}) \rangle$ generically differ, as illustrated in Fig. 4 for five electrons and $S_z = 1/2$. However, as the interaction strength is increased by either suppressing screening (left panel) or increasing the dot size (right panel), the radial profiles of $\langle n_\uparrow \rangle$ (solid lines) and $\langle n_\downarrow \rangle$ (dashed lines) tend to overlap and form the same probability density ring [29]. The rationale is that Coulomb forces localize electrons in space, depleting the probability weight in the

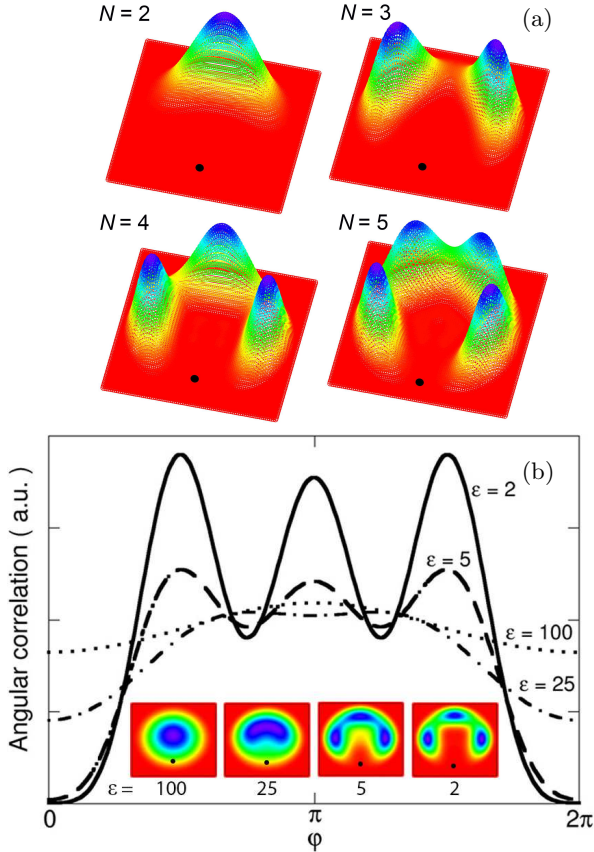


Figure 5. (color online). Polygonal Wigner molecules. (a) Three-dimensional contour plots of $P(\mathbf{r}, \mathbf{r}_0)$ for $\epsilon = 2$ and $R = 2250 \text{ \AA}$. Black dots point to the locations \mathbf{r}_0 of fixed electrons. (b) $P(\mathbf{r}, \mathbf{r}_0)$ vs φ with $|\mathbf{r}| = |\mathbf{r}_0|$ for four electrons and different values of ϵ , with $R = 500 \text{ \AA}$. Inset: corresponding contour plots of $P(\mathbf{r}, \mathbf{r}_0)$ in the xy plane.

regions halfway an electron and its neighbors. Therefore, exchange interactions between pairs of electrons are suppressed, making spin degrees of freedom redundant.

To detect whether angular correlations are enforced by interactions we break the circular symmetry of the one-body density introducing the pair correlation function $P(\mathbf{r}, \mathbf{r}_0)$, i.e., the conditional probability of finding an electron at \mathbf{r} provided another electron is located at the fixed position \mathbf{r}_0 displaced from the origin,

$$P(\mathbf{r}, \mathbf{r}_0) = \frac{1}{N(N-1)} \sum_{i,j=1}^N \langle \delta(\mathbf{r} - \mathbf{r}_i) \delta(\mathbf{r}_0 - \mathbf{r}_j) \rangle_\psi. \quad (6)$$

For the sake of simplicity, here we take the quantum average $\langle \dots \rangle_\psi$ over a selected pure quantum state ψ belonging to the ground-state multiplet and show the sublattice component with the largest weight.

The insets of Fig. 5(b) show how the contour plots of $P(\mathbf{r}, \mathbf{r}_0)$ for four electrons evolve in the xy plane as screening is suppressed. The black dots highlight the positions \mathbf{r}_0 of the fixed electron, located at the maximum of the one-body density with arbitrary angle. As the interaction strength increases [panels from left ($\epsilon = 100$) to

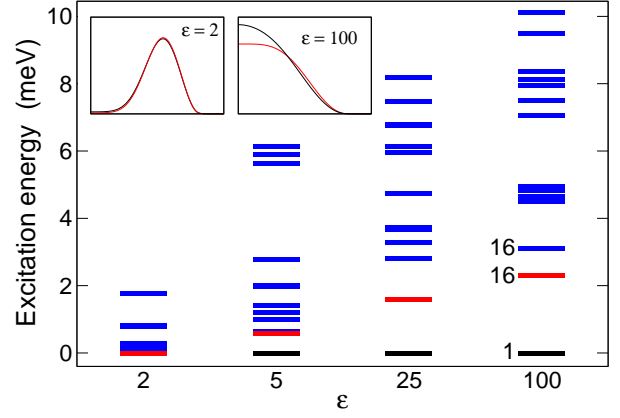


Figure 6. (color online) Excitation spectrum of a Wigner molecule. Low-lying excitation energies vs ϵ for $N = 4$ and $R = 500 \text{ \AA}$. Numbers label degeneracies of selected multiplets. Insets: density $n(\mathbf{r})$ vs ρ averaged over the ground state (black curve) and the first excited multiplet (red [gray] curve).

right ($\epsilon = 2$)], we see—beyond the onset of the correlation hole around the fixed particle—a strong rearrangement of the probability weight: a non-trivial structure emerges made of three peaks located at the vertices of a square whose last vertex is placed at \mathbf{r}_0 . Overall, the three peaks plus the fixed electron realize a square Wigner molecule, which rotates together with \mathbf{r}_0 .

Cutting the contour plots of $P(\mathbf{r}, \mathbf{r}_0)$ along a ring of radius $|\mathbf{r}_0|$ allows us to appreciate the role of interactions in driving spatial order and localization, as we show in Fig. 5(b). For weak correlations (dotted line) P vs φ is featureless, exhibiting a minor depression close to $\varphi = 0, 2\pi$, which realizes the exchange hole around the fixed electron position. Increasing the interaction (up to $\epsilon = 2$, solid line) the three peaks of the square Wigner molecule emerge together with a deep correlation hole around \mathbf{r}_0 , the peak-to-valley ratio increasing with decreasing ϵ .

Figure 5(a) shows the generic behavior of N electrons in the strongly correlated limit, here enforced with $\epsilon = 2$ and $R = 2250 \text{ \AA}$. The electrons realize Wigner molecules whose forms are regular polygons with N vertices, as illustrated by the three-dimensional plots of $P(\mathbf{r}, \mathbf{r}_0)$ for the dimer ($N = 2$), the triangle ($N = 3$), the square ($N = 4$), and the pentagon ($N = 5$).

The excitation spectrum of a Wigner molecule may be measured by either non-linear Coulomb blockade spectroscopy [31]—opening the source-drain bias window in the setup of Fig. 1(a)—or inelastic light scattering [29, 30]. Figure 6 shows the dependence of low-lying excitation energies on the interaction strength for four electrons. For weak interactions ($\epsilon = 100$), the spectrum reminds us of the single-particle ladder of levels of Fig. 1(c), as to excite the ground state one moves an electron from the lowest completely filled shell to higher orbital states. Whereas in this specific case the ground state is non

degenerate, the excited multiplets exhibit large degeneracies (labeled by numbers) linked to different (iso)spin orientations. For stronger interactions, the lowest excitation energies are strongly quenched as the system turns into a square Wigner molecule. Comparing the one-body density $n(\mathbf{r})$ of the ground-state (black curves in the insets) with $n(\mathbf{r})$ averaged over the lowest excited multiplet (red [gray] curves), we see that the two curves overlap for strong interactions (left inset, $\epsilon = 2$). In fact, in the limit of perfect localization the Wigner-molecule ground state exhibits a huge degeneracy since localized electrons may independently flip their (iso)spins, as exchange interactions are completely suppressed. Therefore, the energy spectrum of the Wigner molecule is a ladder of highly-degenerate rovibrational quanta [27, 29, 30].

In conclusion, electrons in a disorder-free graphene quantum dot with a mass gap form Wigner molecules for a broad range of device parameters. The signatures of Wigner localization may be traced in Coulomb blockade and other electron spectroscopies. We expect our findings to be generic to clean carbon-based nanostructures exhibiting a mass gap, including atomically precise ribbons and bilayer-graphene quantum dots.

We thank Elisa Molinari, Deborah Prezzi, Marco Polini, Andrea Candini, Andrea Ferretti, Vittorio Pellegrini, Stefano Corni, and Pino D'Amico for stimulating discussions. This work is supported by MIUR-PRIN2012 MEMO, EU-FP7 Marie Curie initial training network INDEX, CINECA-ISCRA grants IscrC_TUN1DFEW and IscrC_TRAP-DIP.

* massimo.rontani@nano.cnr.it; www.nano.cnr.it

- [1] A. H. Castro Neto, F. Guinea, N. M. R. Peres, K. S. Novoselov, and A. K. Geim, *Rev. Mod. Phys.* **81**, 109 (2009)
- [2] D. S. L. Abergel, V. Apalkov, J. Berashevich, K. Ziegler, and T. Chakraborty, *Adv. Phys.* **59**, 261 (2010)
- [3] S. Das Sarma, S. Adam, E. H. Hwang, and E. Rossi, *Rev. Mod. Phys.* **83**, 407 (2011)
- [4] V. N. Kotov, B. Uchoa, V. M. Pereira, F. Guinea, and A. H. Castro Neto, *Rev. Mod. Phys.* **84**, 1067 (2012)
- [5] P. Recher and B. Trauzettel, *Nanotechnology* **21**, 302001 (2010)
- [6] A. V. Rozhkov, G. Giavaras, Y. P. Bliokh, V. Freilikher, and F. Nori, *Phys. Rep.* **503**, 77 (2011)
- [7] J. Güttinger, F. Molitor, C. Stampfer, S. Schnez, A. Jacobsen, S. Dröscher, T. Ihn, and K. Ensslin, *Rep. Prog. Phys.* **75**, 126502 (2012)
- [8] D. Prezzi, D. Varsano, A. Ruini, A. Marini, and E. Molinari, *Phys. Rev. B* **77**, 041404(R) (2008)
- [9] O. V. Yazyev, *Rep. Prog. Phys.* **73**, 056501 (2010)
- [10] X. Wang, Y. Ouyang, L. Jiao, H. Wang, L. Xie, and J. Wu, *Nature Nanotech.* **6**, 563 (2011)
- [11] D.-K. Ki and A. F. Morpurgo, *Phys. Rev. Lett.* **108**, 266601 (2012)
- [12] M. Müller, J. Schmalian, and L. Fritz, *Phys. Rev. Lett.* **103**, 025301 (2009)
- [13] D. C. Elias, R. V. Gorbachev, A. S. Mayorov, S. V. Morozov, A. A. Zhukov, P. Blake, L. A. Ponomarenko, I. V. Grigorieva, K. S. Novoselov, F. Guinea, and A. K. Geim, *Nature Phys.* **7**, 701 (2011)
- [14] J. Chae, S. Jung, A. F. Young, C. R. Dean, L. Wang, Y. Gao, K. Watanabe, T. Taniguchi, J. Hone, K. L. Shepard, P. Kim, N. B. Zhitenev, and J. A. Stroscio, *Phys. Rev. Lett.* **109**, 116802 (2012)
- [15] D. A. Siegel, W. Regan, A. V. Fedorov, A. Zettl, and A. Lanzara, *Phys. Rev. Lett.* **110**, 146802 (2013)
- [16] A. Bostwick, F. Speck, T. Seyller, K. Horn, M. Polini, R. Asgari, A. H. MacDonald, and E. Rotenberg, *Science* **328**, 999 (2010)
- [17] D. V. Khveshchenko, *Phys. Rev. Lett.* **87**, 246802 (2001)
- [18] J. E. Drut and T. A. Lähde, *Phys. Rev. Lett.* **102**, 026802 (2009)
- [19] N. W. Ashcroft and N. D. Mermin, *Solid State Physics* (Holt-Saunders Intl, New York, NY, 1976)
- [20] H. P. Dahal, Y. N. Joglekar, K. S. Bedell, and A. V. Balatsky, *Phys. Rev. B* **74**, 233405 (2006)
- [21] T. Ando, A. B. Fowler, and F. Stern, *Rev. Mod. Phys.* **54**, 437 (1982)
- [22] E. Wigner, *Phys. Rev.* **46**, 1002 (1934)
- [23] X. Du, I. Skachko, F. Duerr, A. Luican, and E. Y. Andrei, *Nature (London)* **462**, 192 (2009)
- [24] K. I. Bolotin, F. Ghahari, M. D. Shulman, H. L. Stormer, and P. Kim, *Nature (London)* **462**, 196 (2009)
- [25] E. McCann and M. Koshino, *Rep. Prog. Phys.* **76**, 056503 (2013)
- [26] H. Min, R. Bistritzer, J. Su, and A. H. MacDonald, *Phys. Rev. B* **78**, 121401(R) (2008)
- [27] S. M. Reimann and M. Manninen, *Rev. Mod. Phys.* **74**, 1283 (2002)
- [28] C. Ellenberger, T. Ihn, C. Yannouleas, U. Landman, K. Ensslin, D. Driscoll, and A. C. Gossard, *Phys. Rev. Lett.* **96**, 126806 (2006)
- [29] S. Kalliakos, M. Rontani, V. Pellegrini, C. P. Garcia, A. Pinczuk, G. Goldoni, E. Molinari, L. N. Pfeiffer, and K. W. West, *Nature Phys.* **4**, 467 (2008)
- [30] A. Singha, V. Pellegrini, A. Pinczuk, L. N. Pfeiffer, K. W. West, and M. Rontani, *Phys. Rev. Lett.* **104**, 246802 (2010)
- [31] S. Pecker, F. Kuemmeth, A. Secchi, M. Rontani, D. C. Ralph, P. L. McEuen, and S. Ilani, *Nature Phys.* **9**, 576 (2013)
- [32] P. Ruffieux, J. Cai, N. C. Plumb, L. Patthey, D. Prezzi, A. Ferretti, E. Molinari, X. Feng, K. Müllen, C. A. Pignedoli, and R. Fasel, *ACS Nano* **6**, 6930 (2012)
- [33] M. T. Allen, J. Martin, and A. Yacoby, *Nature Commun.* **3**, 934 (2012), doi:10.1038/ncomms1945
- [34] A. M. Goossens, S. C. M. Driessen, T. A. Baart, K. Watanabe, T. Taniguchi, and L. M. K. Vandersypen, *Nano Lett.* **12**, 4656 (2012)
- [35] A. Müller, B. Kaestner, F. Hohls, T. Weimann, K. Pierz, and H. W. Schumacher, "Bilayer graphene quantum dot defined by topgates," (2013), arXiv:1304.7661
- [36] M. Zarenia, B. Partoens, T. Chakraborty, and F. M. Peeters, *Phys. Rev. B* **88**, 245432 (2013)
- [37] P. Recher, J. Nilsson, G. Burkard, and B. Trauzettel, *Phys. Rev. B* **79**, 085407 (2009)
- [38] G. Giovannetti, P. A. Khomyakov, G. Brocks, P. J. Kelly, and J. van den Brink, *Phys. Rev. B* **76**, 073103 (2007)
- [39] B. Hunt, J. D. Sanchez-Yamagishi, A. F. Young,

- M. Yankowitz, B. J. LeRoy, K. Watanabe, T. Taniguchi, P. Moon, M. Koshino, P. Jarillo-Herrero, and R. C. Ashoori, *Science* **340**, 1427 (2013)
- [40] C. R. Woods, L. Britnell, A. Eckmann, R. S. Ma, J. C. Lu, H. M. Guo, X. Lin, G. L. Yu, Y. Cao, R. V. Gorbachev, A. V. Kretinin, J. Park, L. A. Ponomarenko, M. I. Katsnelson, Y. N. Gornostyrev, K. Watanabe, T. Taniguchi, C. Casiraghi, H. Gao, A. K. Geim, and K. S. Novoselov, *Nature Phys.*, doi:10.1038/nphys2954(2014)
- [41] S. Y. Zhou, G. H. Gweon, A. V. Fedorov, P. N. First, W. A. de Heer, D. Lee, F. Guinea, A. H. Castro Neto, and A. Lanzara, *Nature Mater.* **6**, 770 (2007)
- [42] C. R. Dean, A. F. Young, I. Meric, C. Lee, L. Wang, S. Sorgenfrei, K. Watanabe, T. Taniguchi, P. Kim, K. L. Shepard, and J. Hone, *Nature Nanotech.* **5**, 722 (2010)
- [43] J. Xue, J. Sanchez-Yamagishi, D. Bulmash, P. Jacquod, A. Deshpande, K. Watanabe, T. Taniguchi, P. Jarillo-Herrero, and B. J. LeRoy, *Nature Materials* **10**, 282 (2011)
- [44] R. Decker, Y. Wang, V. W. Brar, W. Regan, H. Tsai, Q. Wu, W. Gannett, A. Zettl, and M. F. Crommie, *Nano Letters* **11**, 2291 (2011)
- [45] L. Vitali, C. Riedl, R. Ohmann, I. Brihuega, U. Starke, and K. Kern, *Surface Science* **602**, L127 (2008)
- [46] E. Rotenberg, A. Bostwick, T. Ohta, J. L. McChesney, T. Seyller, and K. Horn, *Nature Mater.* **7**, 258 (2008)
- [47] S. Y. Zhou, D. A. Siegel, A. V. Fedorov, F. El Gabaly, A. K. Schmid, A. H. Castro Neto, D. Lee, and A. Lanzara, *Nature Mater.* **7**, 259 (2008)
- [48] B. Wunsch, T. Stauber, and F. Guinea, *Phys. Rev. B* **77**, 035316 (2008)
- [49] I. Romanovsky, C. Yannouleas, and U. Landman, *Phys. Rev. B* **79**, 075311 (2009)
- [50] A. D. Güçlü, P. Potasz, O. Voznyy, M. Korkusinski, and P. Hawrylak, *Phys. Rev. Lett.* **103**, 246805 (2009)
- [51] P. Potasz, A. D. Güçlü, A. Wójs, and P. Hawrylak, *Phys. Rev. B* **85**, 075431 (2012)
- [52] T. Paananen, R. Egger, and H. Siedentop, *Phys. Rev. B* **83**, 085409 (2011)
- [53] N. Yang and J.-L. Zhu, *J. Phys.: Condens. Matter* **24**, 215303 (2012)
- [54] D. P. DiVincenzo and E. J. Mele, *Phys. Rev. B* **29**, 1685 (1984)
- [55] W. Greiner, B. Müller, and J. Rafelski, *Quantum Electrodynamics of Strong Fields* (Springer Verlag, Berlin, 1985)
- [56] W. Häusler and R. Egger, *Phys. Rev. B* **80**, 161402(R) (2009)
- [57] A. L. Walter, A. Bostwick, K.-J. Jeon, F. Speck, M. Ostler, T. Seyller, L. Moreschini, Y.-J. Chang, M. Polini, R. Asgari, A. H. MacDonald, K. Horn, and E. Rotenberg, *Phys. Rev. B* **84**, 085410 (2011)
- [58] C. Hwang, D. A. Siegel, S.-K. Mo, W. Regan, A. Ismach, Y. Zhang, A. Zettl, and A. Lanzara, *Sci. Rep.* **2**, 590 (2012)
- [59] K. Ohno, *Theor. Chim. Acta* **2**, 219 (1964)
- [60] A. Secchi and M. Rontani, *Phys. Rev. B* **82**, 035417 (2010)
- [61] A. Secchi and M. Rontani, *Phys. Rev. B* **88**, 125403 (2013)
- [62] M. Rontani, C. Cavazzoni, D. Bellucci, and G. Goldoni, *J. Chem. Phys.* **124**, 124102 (2006)
- [63] L. P. Kouwenhoven, C. M. Marcus, P. L. McEuen, S. Tarucha, R. M. Westervelt, and N. S. Wingreen, "Electron transport in quantum dots," (Kluwer, 1997) p. 105
- [64] S. Tarucha, D. G. Austing, T. Honda, R. J. van der Hage, and L. P. Kouwenhoven, *Phys. Rev. Lett.* **77**, 3613 (1996)
- [65] A. Secchi and M. Rontani, *Phys. Rev. B* **80**, 041404(R) (2009)